Fuel 425 (2026) 139458

Contents lists available at ScienceDirect

Fuel

journal homepage: www.elsevier.com/locate/jfue

Full length article

Steering methanol premixed dual-fuel combustion with boundary conditions: Performance gains and mode shifts in a marine engine

Konstantinos I. Kiouranakis [a,*], Robbert Willems [b], Peter de Vos [a], Rinze Geertsma [a,c]

[a] Faculty of Mechanical Engineering, Delft University of Technology, Mekelweg 2, Delft, 2628 CD, the Netherlands
[b] Powertrains Department, Netherlands Organisation for Applied Scientific Research (TNO), Helmond, the Netherlands
[c] Faculty of Military Sciences, Netherlands Defence Academy, Den Helder, the Netherlands

HIGHLIGHTS

- Retrofit-friendly control levers enhance premixed methanol dual fuel engines' performance.
- Diagnostic framework links boundary conditions to engine behavior at high methanol ratios.
- Heat release mapping proves highly effective for combustion control.
- Lower intake pressure improves combustion efficiency with minimal heat-loss penalty.
- Hot residuals promote methanol oxidation during flame propagation.

ARTICLE INFO

Keywords:
Diesel engine
Dual-fuel engine
Heavy-duty
Retrofit
Methanol
Combustion mode
Residual gas

ABSTRACT

Methanol premixed dual-fuel (PRDF) concepts can accelerate shipping defossilization, yet high methanol energy fraction (MEF) operation is often limited by combustion losses and knock behavior. The understanding of how boundary conditions—especially those accessible through retrofit-friendly control levers—influence the performance of methanol PRDF engines remains limited and impedes their high-MEF operation. This paper analyzes results from experiments on a marine-scale single-cylinder methanol PRDF engine at high load and high MEFs. The experiments established the influence of air excess ratio and trapped residual gases on combustion modes, efficiency, and emissions by adjusting the intake and exhaust pressures, respectively. A combined quantitative-qualitative analysis, including heat release morphology mapping, was used to link combustion behavior to performance and emissions. Decreasing intake pressure—richer operation via reduced air excess ratio—substantially improves combustion efficiency with only marginal compromise in heat losses. Increasing exhaust pressure leads to a weaker change in heat release shape than intake pressure, yet it achieves comparable gains in combustion efficiency by retaining hotter residual gas (RG) that promotes methanol combustion during the flame propagation-dominated stage. Heat release morphology shows stronger sensitivity to intake pressure for the sweeps conducted in this study, transitioning from single-peak and bell-shaped to double-peak and h-shaped profiles with increasing intake pressure. This transition indicates a shift from premixed autoignition toward flame propagation. Therefore, retrofit-friendly control levers can steer combustion mode and improve efficiency in high-MEF methanol PRDF operation. As such, this work provides a basis for design-of-experiment-driven optimization and control development.

1. Introduction

Methanol-fueled reciprocating internal combustion engines (ICEs) represent a pivotal technology in the transition toward a renewable future for the off-road transportation industry [1,2]. As global trade relies heavily on shipping, which accounts for a significant share of total greenhouse gas (GHG) and other harmful emissions, the adoption of low-carbon and potentially fully renewable fuels like methanol is essential for achieving defossilization targets [3,4]. Methanol's advantages—including scalable renewable production, good combustion properties, and compatibility with existing infrastructure due to its liquid state at

* Corresponding author.
Email address: K.I.Kiouranakis@tudelft.nl (K.I. Kiouranakis).

https://doi.org/10.1016/j.fuel.2026.139458
Received 13 February 2026; Received in revised form 27 March 2026; Accepted 10 April 2026
Available online 15 April 2026

Abbreviations

aHRR	apparent Heat Release Rate
aTDC	after Top Dead Center
bTDC	before Top Dead Center
CA	Crank Angle
CD	Combustion Duration
CMI	Combustion Mechanism Index
CO	Carbon Monoxide
COV	Coefficient of Variance
DFDC	Dual Fuel Diffusion Combustion
EOC	End of Combustion
EVO	Exhaust Valve Open
gIMEP	gross Indicated Mean Effective Pressure
RGF	Residual Gas Fraction
HD	Heavy-duty
TDC	Top Dead Center
UHC	Unburned Hydrocarbon
ICE	Internal Combustion Engine
ID	Ignition Delay
ITE	Indicated Thermal Efficiency
IVC	Inlet Valve Closing
LRF	Low Reactivity Fuel
CR	Compression Ratio
MEF	Methanol Energy Fraction
DF	Dual Fuel
DO	Diesel-only
NO_x	Nitrogen Oxides
PMR	Phase Magnitude Ratio
PRDF	Premixed Dual Fuel
SOC	Start of Combustion
SOI	Start of Injection
HRF	High Reactivity Fuel
HRR	Heat Release Rate

atmospheric conditions—position it as a viable alternative to fossil fuels, particularly in marine applications, where electrification faces practical limitations [5,6]. By having the potential to maintain high efficiencies and reduce emissions in marine ICEs, methanol can support the fourth propulsion revolution, bridging the gap between current diesel dominance and carbon-neutral operation [7].

Dual-fuel engine technology is currently regarded as the most effective pathway to deploy methanol in marine diesel engines, because it preserves the operating flexibility required in the off-road sector [8]. The more complex dual-fuel diffusion combustion (DFDC) concept is the primary choice for using methanol in large marine engines. However, DFDC relies on high-pressure methanol injection and a spacious cylinder head, which limit scalability and retrofitting potential across a broad range of engine sizes [9]. In contrast, the premixed dual-fuel (PRDF) strategy—using air path injection of methanol with a diesel pilot for ignition—offers a simpler and more adaptable route across various marine platforms, especially when retrofitting is considered. By lowering peak temperatures and increasing charge homogeneity with PRDF, further reduction of nitrogen oxide (NO_x) and soot emissions can be achieved relative to DFDC. Utilizing PRDF by converting existing diesel engines can also accelerate the experiential learning and design feedback for future dedicated methanol engines [1,10].

Despite these advantages, PRDF engines face persistent challenges with reduced combustion efficiency and knock at higher methanol energy fractions (MEFs) [11,12]. Intrusive hardware modifications may be employed, such as geometric CR changes [13], variable CR technologies [14–17], variable valve actuation [18], or exhaust gas recirculation (EGR) [19,20]. Domínguez et al. [21] employed a single-cylinder research diesel engine incorporating several adjustable control variables, including EGR, to study methanol PRDF operation. Leveraging methanol's cooling effect and high EGR rates, they demonstrated that faster and highly-premixed combustion can be achieved compared to the diesel baseline and result in significantly low NO_x and soot emissions. However, PRDF high-load operation was restricted to 60% MEF due to elevated pressure rise rates derived from the premixed combustion. In a subsequent study by the authors [13], the piston crown was replaced by one with a geometrically similar but smaller bowl to assess the impact of increasing compression ratio (CR) on the performance of the engine. Increasing CR from 16 to 18 and lowering EGR decreased ID of diesel and improved combustion stability. The combustion stability improvement contributed to the increase of maximum MEF to 82%, with the main combustion mechanism shifting to flame propagation in the unburned methanol-air mixture. However, this transition increased combustion duration (CD) and resulted in lower indicated thermal efficiency (ITE) compared to the diesel-only (DO) baseline and the lower CR and MEF PRDF operating points.

PRDF combustion remains anchored in diesel injection strategy, because timing, quantity, and characteristics of diesel injection continue to dictate ignition behavior, heat release phasing, and overall combustion behavior. Wang et al. [22] emphasized the key role of pilot injection timing in their efforts to improve combustion performance under part load in a methanol PRDF engine. Advancing pilot injection, together with higher intake temperatures, increased thermal efficiency beyond that of diesel at 60% MEF. Similarly, Li et al. [23], using a six-cylinder heavy-duty (HD) engine, showed that advancing injection timing or increasing injection pressure significantly improves combustion stability and thermal efficiency. Moreover, Yang et al. [24] used numerical simulations to explore the effects of several injection parameters, such as pressure and spray angle, confirming that delayed injection timing deteriorates combustion and overall efficiency, whereas increased injection angle and pressure enhance them. Srna et al. [25,26] conducted fundamental methane-diesel PRDF combustion studies, showing that pilot injection dynamics critically influence the interaction between pilot and methane combustion, which is corroborated by similar optical access studies of methanol-diesel PRDF combustion [27]. The methane-fueled studies also demonstrated that transitioning from DO to PRDF makes combustion more coupled with in-cylinder boundary conditions such as temperature, oxygen density, and equivalence ratios.

When diesel engines are converted to PRDF operation, precise control of boundary conditions becomes essential to ensure robust operation across the engine map and to enable flexible switching between DO and PRDF modes [27]. However, many existing diesel engines employ conventional, mechanically-controlled injection systems that limit direct manipulation of injection parameters such as timing. In such cases, the importance of retrofit-friendly control levers is amplified. Adjustments to intake or exhaust pressure through throttling, as well as modulation of intake air temperature using charge air cooling [28] or heating [29], offer practical means to influence boundary conditions and combustion behavior without requiring fundamental changes to core engine hardware. Experimental investigations have already demonstrated the impact of these measures. For example, raising intake air temperature has shown its ability to mitigate methanol's strong charge cooling and enhance both ignition and combustion stability in PRDF engines, at both low [30] and high loads [31–33]. Conversely, Dierickx et al. [34] reported only marginal improvements in combustion performance at low loads with elevated intake air temperatures, which, according to the authors, may not justify the complexity and cost of implementing an intake air temperature control system. While DF concepts aim at

minimizing the diesel dependence, most experimental studies are limited to low MEFs, as they face knock challenges. This has resulted in the majority of parametric explorations adopting strategies that reduce in-cylinder mixture reactivity to extend these relatively low MEF limits [11]. Dierickx et al. [34] applied EGR and reduced intake pressure, while Guan et al. [35] used EGR and intake air cooling to suppress MEF limitations caused by high pressure gradients at high loads. In a similar way, the study by Cung et al. [36] delayed the combustion phasing using the control levers of pilot injection timing and EGR to increase the maximum MEF at high loads.

However, recent evidence from experimental studies in large-bore methanol PRDF engines [37,38] challenges this knock-centric paradigm. These findings indicate that, in large-bore engines operating under medium to high load and high MEF conditions, performance limitations arise primarily from poor combustion rather than knock. A preceding study by the authors [39] discussed the two typical MEF regions found under methanol PRDF operation, each bounded by a different mechanism: a low-MEF region limited by knock and incomplete combustion, and a high MEF region at which poor combustion performance becomes the dominant limitation. This revised understanding indicates that strategies should prioritize charge reactivity to enable stable and efficient high-MEF operation in methanol PRDF engines. The fact that different combustion mechanisms constrain high-MEF operation at varying load conditions has led to ambiguity regarding the influence of operating parameters on methanol PRDF engine performance. Consequently, this ambiguity and the overall scarcity of studies under high-MEF PRDF operation—particularly in large-bore engines—restricts our understanding of marine-scale methanol PRDF systems, which operate under distinct regimes characterized by lower speeds and higher power outputs.

To address these gaps, this study conducts controlled sweeps of key boundary conditions—air excess ratio (λ) and residual gas (RG) mass—on a marine-size single-cylinder methanol PRDF engine. Employing the analytical framework of [39], the aim is to better understand how boundary conditions affect ignition dynamics, combustion development, efficiency, and emissions at high MEFs. Although optimization toward maximum MEF with high efficiency and low emissions is beyond the present scope, this work provides mechanistic insights into the influence of individual control parameters. Such understanding informs future optimization strategies and promotes a retrofit-oriented pathway for higher methanol utilization in methanol-fueled PRDF marine engines. Overall, the novelty and contributions of this study can be characterized as threefold: i) it provides systematic high-MEF experiments on a marine-scale engine platform, ii) it explores the effect of boundary conditions on combustion modes, and iii) it analyzes the effects in heat release shapes and links them with engine efficiency and emissions.

2. Experimental setup

2.1. Apparatus

Experimental investigations were conducted using a single-cylinder research diesel engine with a modular design, as established in a prior study by the authors on premixed dual-fuel combustion [39]. This setup enables precise control over operating parameters, making it ideal for the parametric sweeps in this work. A schematic of the engine test bed is presented in Fig. 1.

The engine features a CR of 14:1, with a bore and stroke of 170 mm and 180 mm, respectively, resulting in a total displacement of approximately 4.1 L. These specifications mimic large-bore marine high-speed engines, ensuring relevance to HD applications. Key engine and fuel properties are summarized in Table 1. The diesel fuel system consists of a centrally located injector on the cylinder head, supplied by a mechanical inline pump with a needle opening pressure of 340 bar. For methanol delivery, a dual-port fuel injection system enhances mixture formation, utilizing two Bosch HDEV 5.2 injectors targeting the intake runners. This configuration, selected for improved atomization and high MEF, is powered by a stainless steel plunger pump capable of 150 bar pressure. Fuel flow rates for both diesel and methanol are measured via Coriolis mass flow meters, allowing real-time MEF monitoring. Surge tanks on the intake and exhaust sides dampen pressure fluctuations typical of single-cylinder operation, ensuring stable conditions during

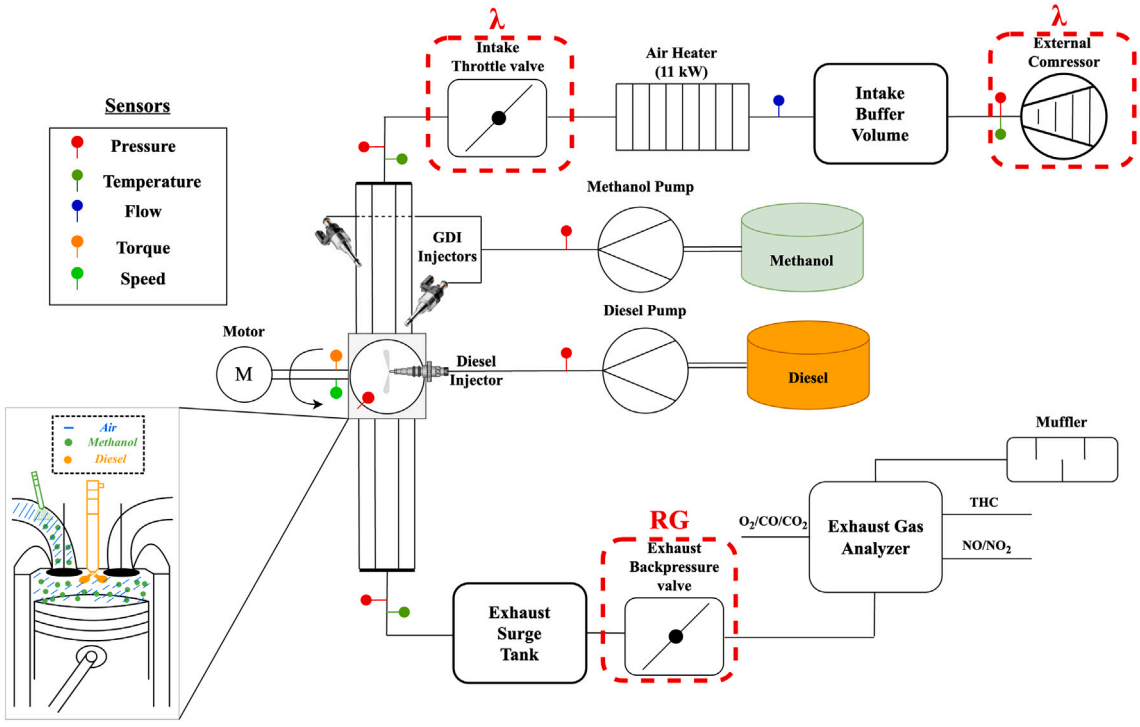

Fig. 1. Schematic diagram of the single-cylinder test setup.

Table 1
Engine and fuel specifications.

Parameter	Specification
Engine	
Type	1-cyl 4-stroke CI
Bore x Stroke [mm]	170×180
Displacement [L]	4.1
Piston bowl shape	ω
Number of valves	4
Compression Ratio [-]	14:1
Fuels	
Diesel type	EN590
Diesel LHV [MJ/kg]	42.7
Diesel HC ratio	1.88:1
Methanol type	ISO 6583 Grade A
Methanol LHV [MJ/kg]	19.9

sweeps. Two valves are also located in the intake and exhaust paths that can adjust the boost and back pressure, enabling the control of air excess ratio and residual gas fraction, respectively. However, in this study, intake pressure sweep results from the compressor speed adjustment alone, with intake throttling used only when pressures below the compressor's minimum air flow capability are required.

2.2. Data acquisition and processing

This experimental campaign aims to collect engine operating data under steady-state conditions. These data are divided into two main categories: 1) slow-speed data, including intake/exhaust manifold pressure and temperature, mass flow rates, and exhaust gas composition, acquired at 10 Hz and averaged over one-minute intervals; and 2) high-speed data, including in-cylinder pressure traces measured by an uncooled 6125C piezoelectric pressure transducer synchronized with a crank angle encoder with 0.1 °CA resolution. In-cylinder pressure was pegged to absolute levels using a two-point polytropic fit applied on a cycle-resolved basis. The crank-angle signal was first referenced to TDC using the encoder and then fine-tuned once, at the beginning of the test campaign, based on a warm motored cycle, ensuring all recorded pressure traces include the corrected TDC offset. Fifty consecutive cycles were processed using a first-order Savitzky-Golay filter with a 2.7°CA frame length to obtain the ensemble-averaged pressure for heat release calculations. Because the analysis focuses on comparative trends and qualitative combustion-mode interpretation rather than on single optimized operating points, these ensemble-averaged traces were considered appropriate for the present purpose.

2.3. Operating test conditions

Employing the thermodynamic-based experimental framework developed in [39], this study extends the analysis by incorporating parametric sweeps of key control parameters: intake and exhaust pressure. Table 2 provides the discrete levels for the different control levers employed in this study. To assess the effect of air excess ratio on engine performance, intake pressure was varied from 1.8 to 2.6 bar. During the sweep, engine speed (1500 rpm), pilot start of injection (SOI) timing ($\approx$ 11°CA bTDC), and MEF (81%) were held constant. As a result, the boost pressure variations induce changes in engine torque and therefore power output. The tested operating range remains centered on a representative high-load point of approximately 15.30 gIMEP, ranging between 15.23 to 15.45 bar. Exhaust pressure was also adjusted to maintain the intake-exhaust scavenging pressure differential $\Delta p = p_{\text{exhaust}} - p_{\text{intake}}$, which also affects retained residual gas (RG). To further isolate the role of RG, a separate exhaust-pressure sweep was conducted from 2.21 to 2.90 bar at 92% MEF, with a SOI of 15°CA bTDC, and an average load of 14.80 bar gIMEP, ranging between 14.47 to 15.10 bar. Injection timing adjustments were carried out by modifying the pump's angular position relative to the engine camshaft. This sweep was also performed at 1500 rpm, with an intake temperature of 318 K (slightly lower than the 323 K used in the intake-pressure sweep). The differences in boundary conditions between the two pressure sweeps stem from their involvement within a broader experimental campaign methodology; however, these variations do not affect the overarching objective of isolating the influence of the targeted boundary conditions on engine performance.

3. Data analysis methodology

This section outlines the methodology employed to investigate the combustion and performance characteristics of a marine single-cylinder engine operating in methanol PRDF mode. The experimental framework relies on the detailed procedures described in a prior study by the authors [39], which serves as the foundational reference for the parametric studies conducted here. Key aspects include engine configuration,

Table 2
Experimental operating points.

Sweep	p_{intake} [bar]	p_{exhaust} [bar]	$\Delta p_{\text{scavenge}}$ [kPa]	gIMEP [bar]	Diesel flow [grams/cycle]	MeOH flow [grams/cycle]	MEF [%]	λ_{global}
Intake pressure	1.80	1.80	0.7	15.26	0.061	0.538	81	1.91
	1.85	1.85	−0.2	15.30	0.061	0.538	81	1.97
	1.90	1.89	−0.7	15.28	0.060	0.538	81	2.03
	1.95	1.95	0.5	15.28	0.060	0.537	81	2.09
	2.00	2.00	0.2	15.27	0.060	0.539	82	2.15
	2.05	2.04	−1.2	15.40	0.061	0.539	81	2.20
	2.10	2.11	0.4	15.35	0.060	0.542	82	2.25
	2.16	2.16	−0.1	15.36	0.061	0.542	82	2.30
	2.21	2.22	0.3	15.45	0.062	0.544	81	2.34
	2.27	2.27	−0.2	15.23	0.062	0.545	81	2.40
	2.31	2.32	0.4	15.40	0.063	0.547	81	2.44
	2.37	2.39	1.2	15.39	0.063	0.551	81	2.48
	2.53	2.54	1.1	15.36	0.063	0.565	81	2.60
	2.59	2.58	−5.4	15.34	0.063	0.570	82	2.62
Exhaust pressure	2.22	2.21	−1.1	14.47	0.026	0.602	92	2.46
	2.22	2.32	9.9	14.74	0.027	0.602	92	2.45
	2.21	2.44	23.2	14.65	0.026	0.602	92	2.45
	2.22	2.52	30.7	14.76	0.027	0.602	92	2.44
	2.21	2.60	39.0	14.99	0.028	0.602	92	2.43
	2.21	2.70	50.0	14.85	0.027	0.601	92	2.44
	2.23	2.80	58.3	15.10	0.028	0.600	92	2.43
	2.22	2.90	69.0	15.04	0.027	0.602	92	2.43

fuel introduction strategies, air to fuel ratio definitions, and combustion analysis frameworks.

3.1. Boundary conditions

For the closed-cycle thermodynamic analysis, the trapped mass, charge composition, and temperature at inlet valve closing (IVC) are required boundary conditions. The inducted air and fuel masses are obtained from measured flow data, while the residual gas mass is estimated using a simplified Mirsky approach, assuming isentropic expansion of the residual gases between exhaust valve opening (EVO) and the end of gas exchange [40]. In this work, the inlet valve opening (IVO) is taken to mark the end of gas exchange, as it occurs slightly earlier than exhaust valve closing (EVC), and the small residual loss during overlap is neglected [41]. The total trapped mass is then determined by summing the estimated residual mass and the measured inducted one, with the temperature at IVC being calculated from the ideal gas law.

3.2. Performance characteristics

Experiments were performed on a marine single-cylinder engine configured for dual-fuel operation. Methanol is introduced via PFI, with a quantity of diesel serving as the pilot fuel for ignition. To quantify the displacement of diesel by methanol, the metric of methanol energy fraction MEF is used:

$$\mathrm{MEF} = \frac{\dot{m}_\mathrm{m} \cdot \mathrm{LHV}_\mathrm{m}}{\dot{m}_\mathrm{m} \cdot \mathrm{LHV}_\mathrm{m} + \dot{m}_\mathrm{d} \cdot \mathrm{LHV}_\mathrm{d}} \cdot 100\% \tag{1}$$

where $\dot{m}$ and LHV are the mass flow rate and lower heating value of each fuel, respectively, and subscripts m and d correspond to methanol and diesel fuel, respectively.

A central focus of this study is the manipulation of the air excess ratio (λ), achieved by varying intake pressure. These adjustments influence critical physical processes, such as pilot fuel breakup and evaporation, as well as chemical kinetics, including diesel autoignition and methanol combustion propagation. In DF systems, defining the air excess ratio is complex due to the differing stoichiometric requirements of the fuels and the stratified nature of the pilot injection, which deviates from the more uniform mixture in conventional spark ignition engines. To address this, three air excess ratio definitions are employed, each aiming to capture different aspects of the combustion process. Global air excess ratio λ_global, providing an overall measure of mixture richness, considers both fuels relative to the total air supply:

$$\lambda_\mathrm{global} = \frac{\dot{m}_\mathrm{air}}{(\dot{m}_\mathrm{m} + \dot{m}_\mathrm{d}) \cdot (\mathrm{MMF} \cdot \mathrm{AFR}_\mathrm{stoich,m} + (1 - \mathrm{MMF}) \cdot \mathrm{AFR}_\mathrm{stoich,d})} \tag{2}$$

where $\dot{m}_\mathrm{air}$ is the mass flow rate of air, and $\mathrm{AFR}_\mathrm{st,i}$ is the stoichiometric air-to-fuel ratio for each fuel. Methanol air excess ratio λ_MeOH, approximating the premixed charge conditions for flame propagation, focusing solely on methanol and air:

$$\lambda_\mathrm{m} = \frac{\dot{m}_\mathrm{air}}{\dot{m}_\mathrm{m} \cdot \mathrm{AFR}_\mathrm{st,m}} \tag{3}$$

Defining an air excess ratio specifically for diesel combustion is challenging due to the high degree of stratification. This study employs the simplistic approach of oxygen reservation by methanol to define a single metric for diesel air excess ratio:

$$\lambda_\mathrm{d} = \frac{\dot{m}_\mathrm{air} - \mathrm{AFR}_\mathrm{st,m} \cdot \dot{m}_\mathrm{m}}{\dot{m}_\mathrm{d} \cdot \mathrm{AFR}_\mathrm{st,d}} \tag{4}$$

3.3. Dual analytical combustion framework

Combustion characteristics are quantified through pressure-based heat release analysis grounded in the first law of thermodynamics. The fundamental basis of this assessment is the apparent heat release rate (aHRR), calculated from highly-resolved in-cylinder pressure data. For energy balance analysis, heat transfer losses are estimated using the Woschni correlation [42] and calibrated with the measured exhaust gas composition, while the gross indicated work is obtained directly from the in-cylinder pressure measurements. For calibration purposes and the estimation of combustion efficiency, unburned hydrocarbon (UHC) emissions were derived from the FID channel of the Horiba MEXA-ONE system and, for methanol operation, were interpreted predominantly as unburned methanol using a constant methanol response factor of 0.63 across all points. The exhaust losses are determined by closing the energy balance. Different combustion phases are denoted as CAx, representing the crank angle position at which a specified percentage of cumulative aHRR is achieved.

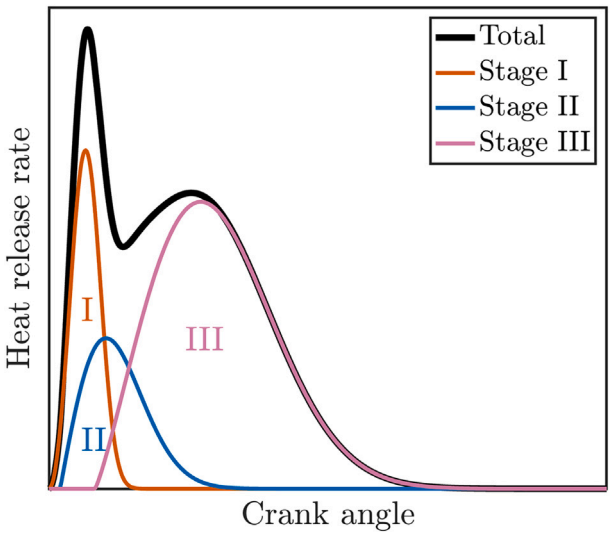

Fig. 2. Dual-fuel conceptual model defining three main combustion stages (based on [43,48]).

This work applies a dual analytical framework to analyze combustion [39]. The first part of the analysis seeks to qualitatively elucidate the distinct combustion processes found in the intricate reaction environment of PRDF engines. As each combustion mechanism is expected to influence energy release characteristics uniquely, this research intends to identify and clarify them with the purpose of better understanding their interplay and impact on engine performance. While this pressure-based HRR analysis alone cannot provide full mechanistic resolution of such combustion phenomena, the analysis incorporates a combination of physical interpretation of combustion stages and fundamental combustion insights from prior PRDF engine studies [27,43–47]. To characterize DF combustion, this study uses an adapted version of the conceptual DF model of Karim, dividing the combustion process into three stages (see Fig. 2):

- **Stage I:** Premixed autoignition of the pilot fuel, including entrainment of low-reactivity fuel (LRF).
- **Stage II:** Premixed autoignition in the LRF-air mixture.
- **Stage III:** Bulk turbulent flame propagation through the LRF-air mixture, including any remaining diesel diffusion burning.

This stage-wise theoretical description of heat release profiles provides groundwork for comprehensive mode evaluation in PRDF combustion [39].

To further support the qualitative analysis and enable a more systematic combustion mode identification, this study employs two heat release morphology metrics, as shown in Fig. 3, which quantify the shaping characteristics of the HRR profile:

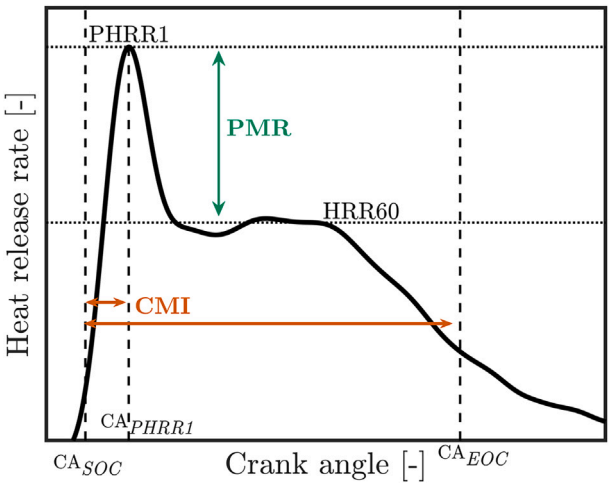

Fig. 3. Shaping characterization methodology using CSI and PMR.

- **Combustion Mechanism Index (CMI):**

$$\mathrm{CMI} = \frac{\mathrm{CA_{PHRR1}} - \mathrm{CA_{SOC}}}{\mathrm{CA_{EOC}} - \mathrm{CA_{SOC}}} \cdot 100\% \tag{5}$$

where $\mathrm{CA_{PHRR1}}$, $\mathrm{CA_{SOC}}$, $\mathrm{CA_{EOC}}$ represent crank angles of the first peak of HRR, start of combustion, and end of combustion, respectively.

- **Phase Magnitude Ratio (PMR):**

$$\mathrm{PMR} = \frac{\mathrm{PHRR1}}{\mathrm{HRR60}} \cdot 100\% \tag{6}$$

where PHRR1 represents the first peak in HRR and HRR60 denotes HRR at CA60.

CMI and PMR metrics enable classification of HRR profiles by directly linking shape features to the underlying combustion mechanisms [39]. Applying this methodology to datasets from two MEF sweeps at high loads demonstrated that PMR-CMI mapping can systematically classify profiles according to their mechanism and phasing characteristics, dividing the map into quadrants, as shown in Fig. 4. Each quadrant, defined by specific set ranges of CMI and PMR, corresponds to a distinct combustion behavior characterized by these two values:

- Quadrant I (CMI > 15%, PMR > 100%): Populated by Mode I (m-shape), this regime reflects strong premixed autoignition for both diesel and methanol, with comparable peak magnitudes and reduced phase separation. Higher CMI values indicate faster combustion, and increasing premixed autoignition behavior that moves operation closer to knock limits.
- Quadrant II (CMI < 80%, PMR > 100%): Populated by Mode II (h-shape), this region is characterized by a dominant pilot autoignition followed by slower methanol flame propagation.
- Quadrant III (CMI < 15%, PMR < 100%): Populated by Mode III (n-shape), this regime is distinguished by a small pilot followed by a stronger methanol flame-propagation. The dominance of flame propagation as the main combustion mechanism leads to greater temporal separation between the diesel and methanol combustion phases, thereby lowering CMIs.
- Quadrant IV (CMI > 15%, PMR < 100%): Not observed experimentally in the preceding experimental study. This regime would theoretically feature two strong HRR peaks with a stronger second phase, indicating enhanced methanol autoignition similar to Mode I.

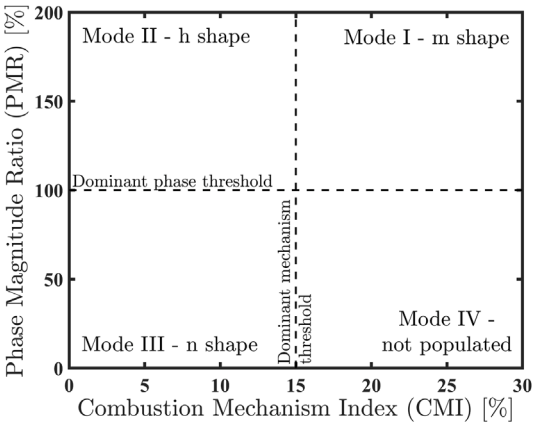

Fig. 4. Heat release profile mapping based on CMI vs PMR metrics.

To quantitatively analyze the combustion phases and distinguish the transition between them, this research uses unique-to-PRDF metrics, derived from correlations between pressure-based HRR features and optical diagnostic studies [48]. The local maxima in the second derivative of the HRR profile are highly correlated with the actual transitions between the combustion phases in a PRDF configuration leading to the phases between the injection event and EOC:

1. **Delay phase (Ignition delay),** which ranges from the start of injection (θ_{SOI}) to the first local maxima of the second derivative of the HRR signal (θ_1) that defines the SOC.
2. **Combustion Phase I (Pilot combustion),** which starts after the ID and lasts until the second local maxima (θ_2), primarily resembling the pilot combustion (Stage I).
3. **Combustion Phase II (Methanol combustion),** which defines the second combustion phase dominated by methanol, ranging from the end of Combustion Phase I to the EOC, taken as the CA90.

As this research uses the terms of combustion *stages* and *phases* extensively, it should be clarified that the term *stages* refers to the mode-informed qualitative analysis of combustion mechanisms, while *phases* denote the two-phase (diesel and methanol) division from the quantitative analysis. In short, across the discussion of results, phases capture the quantitative trends, whereas stages provide with complementary insights not resolved by the quantitative method.

4. Results and discussions

4.1. Effect of intake pressure

Air excess ratio (λ) is the principal boundary condition manipulated along the intake pressure adjustment. This pressure adjustment, however, inherently modifies several interrelated in-cylinder boundary conditions, which together influence combustion dynamics over the closed in-cylinder process period. Fig. 5 illustrates how progressively increased boost pressure drives changes in multiple boundary parameters, including various defined air excess ratios (λ), temperature and pressure at inlet valve closure (IVC) (T_{IVC} and p_{IVC}), specific heat ratio during compression (γ_{comp}), and trapped masses. RG represents the estimated amount of hot exhaust gases retained from the previous cycle.

Despite the expected decreasing trend in RG mass during the intake pressure increase which enhances scavenging efficiency, this study simultaneously adjusted the exhaust pressure throughout the sweep to ensure a nearly constant scavenging pressure differential, as seen in Table 2. As a result, the increasing exhaust pressure together with increasing inertia due to elevated gas densities during the intake pressure increase led to an increase in total trapped RG mass from 0.11 to

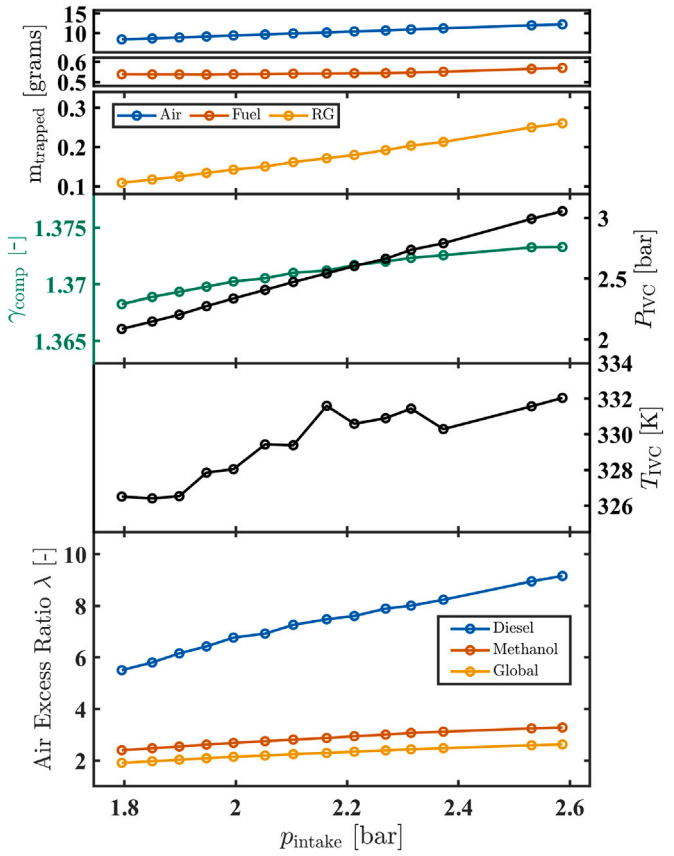

Fig. 5. Boundary condition changes across the intake pressure sweep.

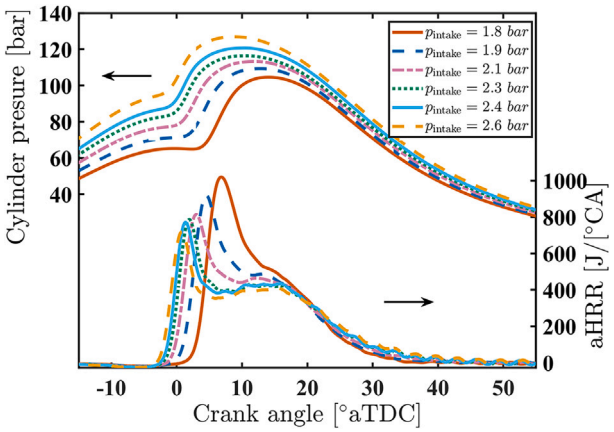

Fig. 6. Effect of intake pressure on in-cylinder pressure and aHRR.

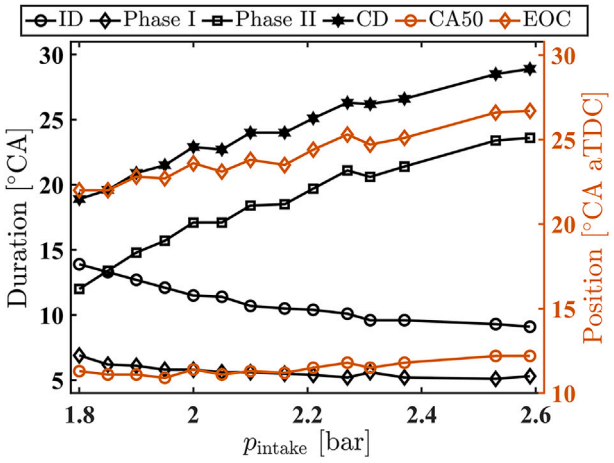

Fig. 7. Effect of intake pressure on combustion phasing and duration.

0.26 grams over the full sweep. Intake charge temperature rose across the boost sweep, reflecting the higher enthalpy input associated with increased air mass, further offsetting methanol's cooling effect. Despite elevated in-cylinder temperatures, the specific heat ratio γ_{comp} also rose, driven by the composition change and the higher specific heat associated with the increased air fraction in the charge. All air excess ratio definitions λ—global, methanol, and diesel-specific—demonstrate an increasing trend with intake pressure, deriving from greater air masses trapped in the cylinder. However, the diesel air excess ratio shows a markedly higher sensitivity to intake pressure variations. The diesel-specific air excess ratio responds more sharply to changes in intake oxygen density, arising from the pronounced difference in stoichiometric air-to-fuel ratios ($AFR_{stoich.}$) between diesel and methanol. This heightened sensitivity crucially influences the pilot fuel's ignition characteristics, and since PRDF combustion dynamics are highly sensitive to ignition delay (ID) and the methanol-pilot fuel interaction, the oxygen availability to diesel plays a critical role in the overall combustion behavior [26,39,49].

Fig. 6 illustrates how increasing intake pressure affects the HRR and in-cylinder pressure profiles. As intake pressure rises, the ID shortens, leading to earlier combustion phasing and elevated in-cylinder pressures throughout the sweep. The lower ID leads to the first part of combustion occurring closer to TDC leading to the increasing trend of peak pressure across the sweep from 105 to 127 bar. This reduction in ID results from several boundary condition changes:

- Elevated intake valve closure temperatures T_{IVC} and overall thermal state.
- Increased λ_d, boosting the oxygen density for the pilot and enhancing mixing.
- Higher in-cylinder pressures during injection due to increased intake valve closure pressures p_{IVC} and specific heat ratio ($\gamma_{comp.}$).

Fig. 7 shows the effects of intake pressure on combustion phasing metrics, quantifying the decreasing trend of ID from 13.9 to 9.1°CA. This shortens Phase I from 6.9 to 5.3°CA, but overall combustion phasing is delayed, as evidenced by later combustion phasing (CA50) and EOC values due to the prolongation of Phase II from 12 to 23.6°CA. With increasing intake pressure, the HRR profile becomes less symmetric, as Phases I and II separate further. The less compact heat release profile at higher intake pressure results in a lower pressure rise rate (PRR) that drops from 7.9 to 7.1 bar/°CA across the sweep. Additionally, the slower combustion phasing deteriorates combustion stability with COV_{gIMEP} rising from 1.1% to 3.2%.

At the lowest intake pressure, the longer ID causes most of the diesel to burn in Stage I, while more methanol combusts either entrained within the pilot fuel (Stage I) or via premixed autoignition near the jets (Stage II). Lower air excess ratios under these conditions also increase reactivity during flame propagation combustion in Stage III, pulling its phasing closer to the first two stages. Fig. 8 summarizes this evolution: Stage I is delayed and grows slightly due to more entrained methanol, Stage II strengthens, and Stage III accelerates, yet with less fuel left to burn. Together these effects improve overall combustion phasing despite the later ignition, and yield the HRR profile observed at lower intake pressures.

Fig. 9 depicts the impact of intake pressure on the distribution of fuel energy across the main energy pathways. Delayed combustion phasing and poor combustion performance remain the main barriers to achieving diesel-like efficiency in methanol PRDF operation—a challenge that becomes even more difficult to overcome when diesel injection timing

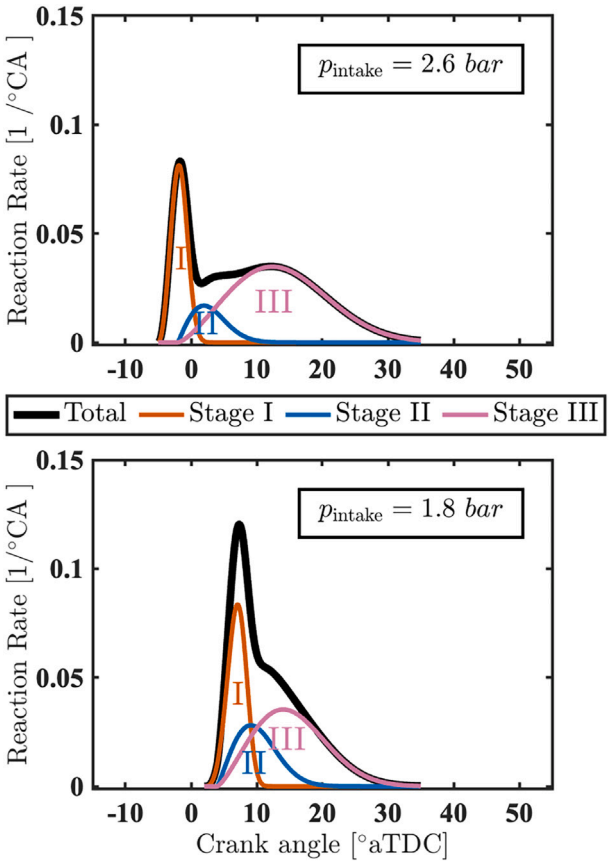

Fig. 8. Conceptual model for the two extreme cases of the intake pressure sweep.

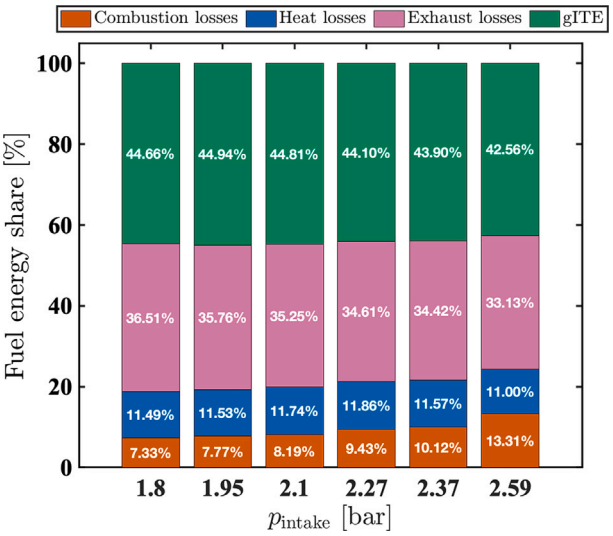

Fig. 9. Effect of intake pressure on fuel's energy distribution.

cannot be readily adjusted, as in this testbed. Combustion efficiency is highly sensitive to intake pressure and its influence on boundary conditions, especially air excess ratio, decreasing from 92.7% at 1.8 bar to 87.7% at 2.6 bar. This improvement at lower intake pressures is attributed to faster flame propagation under richer conditions, resulting in a more compact heat release and a reduced proportion of fuel burning during the second combustion phase. Interestingly, despite the enhanced combustion efficiency at lower intake pressure, heat loss remains nearly

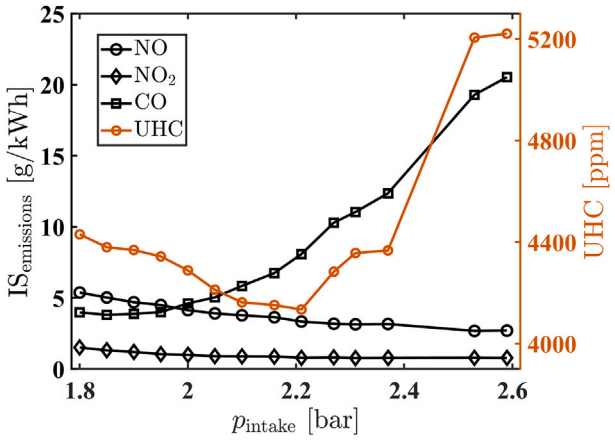

Fig. 10. Effect of intake pressure on emission characteristics.

constant with a slight increase from 11.00% to 11.49%. A shorter combustion duration, advanced phasing, and reduced pressure levels are the primary factors contributing to the heat loss increase offset resulting from the higher temperatures associated with richer combustion under the lower intake pressure conditions. This heat loss effect suggests that enriching the mixture with lower intake pressure offers potential to improve combustion efficiency providing space for further improvement through intake temperature increase or advanced pilot injection. This room for further parametric adjustments can also help decrease the exhaust energy losses that derive from the longer ID at lower intake pressures. However, such parametric adjustments that advance combustion phasing should be implemented cautiously, as they may elevate knocking propensity. Overall, gross indicated thermal efficiency (gITE) clearly improved from 42.56% at the highest pressure to 44.66% at the lowest, demonstrating the potential of intake pressure manipulation to enhance combustion and performance. A comprehensive assessment in a multi-cylinder context, accounting for gas dynamics and pumping losses, is still necessary to draw more holistic conclusions regarding performance improvements.

Fig. 10 shows the effect of intake pressure on the emissions characteristics. In line with the combustion efficiency trends, both UHC and carbon monoxide (CO) emissions generally increase with intake pressure. However, unlike the combustion loss trend, UHC emissions exhibit a non-monotonic behavior—decreasing from 4430 ppm at 1.8 bar to 4162 ppm at 2.1 bar, before rapidly rising to 5221 ppm at 2.6 bar. This apparent inconsistency arises from the different bases of these two quantities. UHC concentration represents the ratio of unburned hydrocarbon molecules to the total exhaust gas molecules, making it dependent on the total exhaust mass flow. Combustion efficiency, on the other hand, reflects only the ratio of released energy to the total fuel energy supplied. As intake pressure increases, the air excess ratio and total exhaust flow rise, partially offsetting the effect of higher unburned fuel on UHC concentration. Thus, while higher combustion efficiency tends to lower UHC emissions, the concurrent decrease in exhaust gas flow can mask this effect, particularly at lower intake pressures where combustion efficiency improvements were more modest.

Nitrogen oxide (NO) and nitrogen dioxide (NO_2) exhibit opposite trends to CO and UHC, consistently decreasing with increasing intake pressure. Specifically, NO drops from 5.38 to 2.70 g/kWh, reflecting the lower combustion temperatures associated with leaner mixtures at higher intake pressures. NO_2 also declines from 1.51 to 0.79 g/kWh across the sweep. This NO_2 behavior can be attributed to the three main factors that favor its rise: 1) density of methanol in the end-gas which can support late combustion oxidation and provide the hydroperoxyl (HO_2) radical, 2) NO density originating from the pilot combustion phase, and 3) suitable temperature levels that support the conversion of

NO to NO_2 [50]. Methanol density remains at similar levels during the intake pressure sweep. The similar levels of methanol quantity in the end gas and the higher end-gas temperature with lower intake pressure, thus HO_2 density, promote the conversion rate of NO to NO_2. Richer combustion of methanol alongside the pilot fuel also results in higher local temperatures, increasing NO formation. Together, these effects promote the reaction $NO + HO_2 \rightarrow NO_2 + OH$, thereby increasing NO_2 at lower intake pressures.

4.2. Effect of exhaust pressure

This section discusses the results from the exhaust pressure sweep which influences the scavenging pressure differential. Compared to the intake pressure sweep, the impact on RG mass was slightly weaker, with trapped RG increasing from 0.18 to 0.21 grams. However, unlike the intake cases, most other boundary conditions remained nearly constant. This configuration was intentionally designed to isolate the influence of residual gas on combustion as a strategy to increase the in-cylinder temperature by retaining more hot RG and providing ignition/combustion assistance. As shown in Fig. 11, RG mass exhibits an increasing trend with rising exhaust pressure, while air mass decreases marginally due to the reduced scavenging efficiency and more trapped RG. While not explicitly shown in the figure, oxygen density is expected to slightly decrease due to this replacement of air by residual gases. T_{IVC} rose from 324 to 328 K across the sweep. Other boundary conditions like air excess ratios and p_{IVC} are not displayed explicitly in Fig. 11 due to their nearly constant values, conserving space.

Fig. 12 depicts the effect of exhaust pressure on the HRR and bulk gas temperature profiles. Two main differences emerge compared to the intake pressure cases: 1) combustion behavior is notably less sensitive to exhaust pressure variations, as anticipated from the smaller impact on boundary conditions; and 2) the baseline HRR profile across the sweep differs distinctly from that of the intake pressure sweep. The HRR differences stem primarily from two factors: the distinct MEFs (81% for intake and 92% for exhaust) and the more advanced injection timing used during the exhaust pressure sweep. To aid the comparison, Fig. 13 presents two representative HRR profiles from the two pressure sweeps which share most boundary conditions: the base intake pressure case of 2.2 bar and the base exhaust pressure case of 2.2 bar. Both operate at comparable load levels and exhibit a minimized scavenging pressure differential between intake and exhaust. However, the intake pressure case shows a stronger premixed combustion Phase I followed by a weaker Phase II, whereas the exhaust pressure case exhibits a less pronounced Phase I and a prolonged Phase II which consumes most of the fuel. In the exhaust-pressure case, the higher MEF weakens the pilot's ignition energy, which—combined with the advanced injection timing that

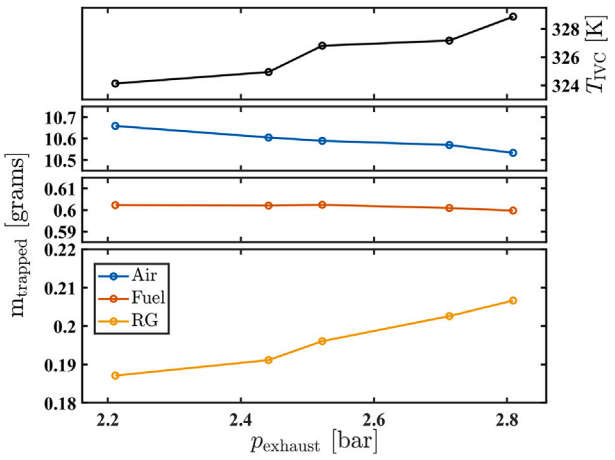

Fig. 11. Effect of exhaust pressure on trapped masses.

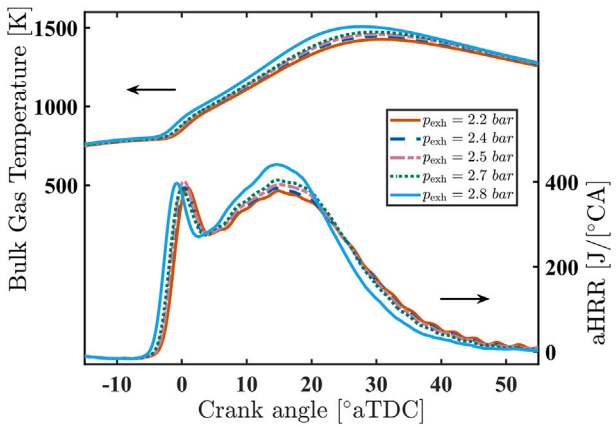

Fig. 12. Effect of exhaust pressure on bulk gas temperature and aHRR.

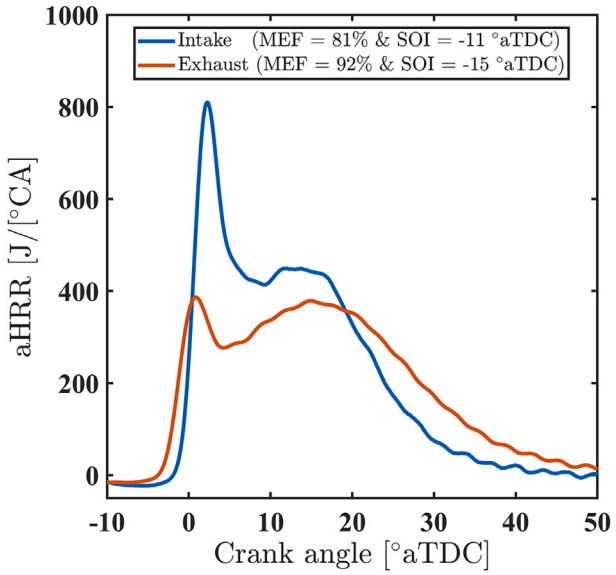

Fig. 13. Comparison of heat release base profiles between intake/exhaust pressure sweeps.

counterbalances a further ID rise—leads to ID reduction, advancing the pilot combustion phasing and enhancing the flame-propagation characteristics of the methanol–air mixture. Overall, despite these distinctions between the two baseline cases, they do not obscure the main objective of this chapter: to isolate and elucidate the influence of specific boundary conditions on methanol PRDF combustion behavior.

Despite the weaker sensitivity of combustion to exhaust pressure sweep compared to the intake, changes still arise in the HRR profile due to variations in RG mass. The increased presence of hot RG enhanced ignition and combustion dynamics by shortening ID and advancing the heat release profile, as corroborated by the combustion phasing metrics in Fig. 14. The ID decreased from 12.2 to 10.9°CA, leading to a slightly shorter Phase I (from 6.2 to 5.9°CA) and an earlier onset of Phase II (from 3.5 to 1.8°CA aTDC). Higher bulk gas temperatures across the sweep further accelerated combustion, shortening Phase II from 28.6 to 26°CA and advancing both CA50 (from 15.8 to 13.9 °CA aTDC) and EOC (from 34.8 to 27.8 °CA aTDC). While the associated reduction in oxygen availability at higher exhaust pressure is expected to prolong ID, the concurrent rise in thermal state due to more hot residual gases dominates the response, resulting in an overall ID reduction. This behavior corroborates the study of Srna et al. [25,26] which demonstrates that, in PRDF mode with methane, the sensitivity of the pilot ID to thermal

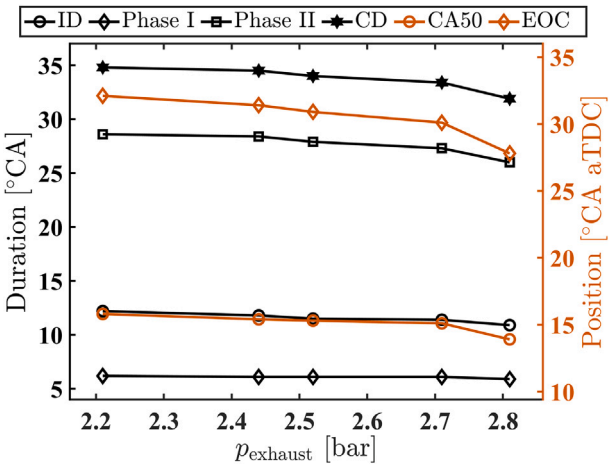

Fig. 14. Effect of exhaust pressure on combustion phasing and duration.

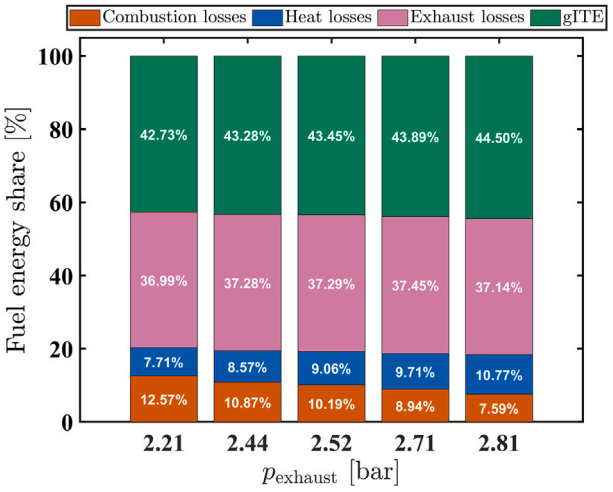

Fig. 15. Effect of exhaust pressure on fuel's energy distribution.

state increases compared to DO mode, while its sensitivity to oxygen density decreases. The stronger sensitivity of EOC compared to CA50 highlights the additional influence of hot RG mass and elevated mixture temperature on the ignition advancement of Phase II combustion, which promoted faster flame propagation through the methanol-air mixture. Overall, the total CD decreased from 34.8 to 31.9°CA.

Fig. 15 shows the effects of exhaust pressure on the fuel energy distribution. Despite the relatively minor impact of exhaust pressure on the HRR profile, the energy balance shows a strong sensitivity of combustion behavior to the increased mass of hot RGs. The combustion efficiency trend reflects the combustion enhancement trend observed in the HRR profiles, rising from 87.34% at the baseline exhaust pressure condition of 2.2 bar to 92.41% at that of 2.8 bar. This confirms that the higher bulk gas temperatures resulting from the trapped hot RGs substantially improved methanol oxidation, particularly under Phase II which is the main contributing factor to incomplete combustion products. This trend is similar to the enhancing effects of intake air temperature observed in the preceding experimental study on this engine [39]. This improvement comes at the expense of slightly higher heat losses, which increased from 7.71% to 10.77%, while exhaust losses remain nearly constant around 37% across the sweep due to the minimal impact of exhaust pressure on combustion phasing. However, the overall combustion enhancement outweighed the rise in heat losses, leading to an improvement in gITE from 42.73% to 44.50%.

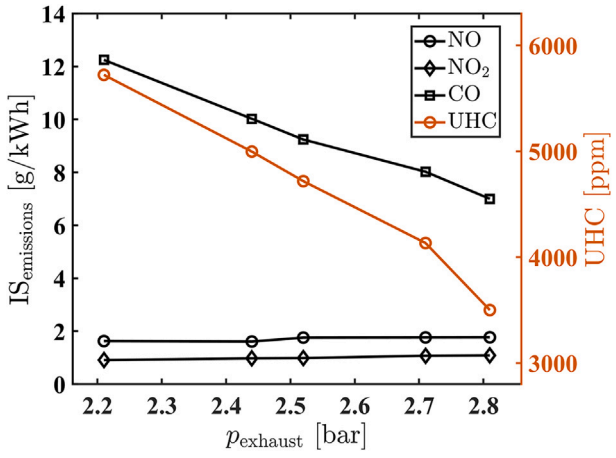

Fig. 16. Effect of exhaust pressure on emissions characteristics.

The combustion improvements are further corroborated by the consistent decrease in UHC emissions, which dropped from 5720 to 3499 ppm, as shown in Fig. 16. CO emissions followed a similar, though less pronounced, decline from 12.25 to 7.00 g/kWh. The smaller reduction in CO compared to UHC emissions can be attributed to the interplay between improved combustion efficiency—which lowers UHC emissions—and the tendency for increased intermediate CO formation with more fuel undergoing partial oxidation before its final conversion to CO_2. Interestingly, despite a 40% rise in heat losses across the sweep, NO emissions increased moderately by about 9% (from 1.63 to 1.77 g/kWh), while NO_2 rose more substantially by 20% (from 0.91 to 1.09 g/kWh). The more modest rise in NO can be linked to reduced oxygen density with higher residual gas content and higher end-gas temperatures which promote more of the formed NO to convert to NO_2 at the later combustion phasing, as discussed earlier for the intake pressure sweep.

4.3. Parametric effects on combustion mode characteristics

As described in [39], an earlier investigation identified three distinct combustion modes through qualitative heat release analysis, each characterized by a specific HRR profile linked to the underlying combustion mechanisms. To support this analysis, two quantitative

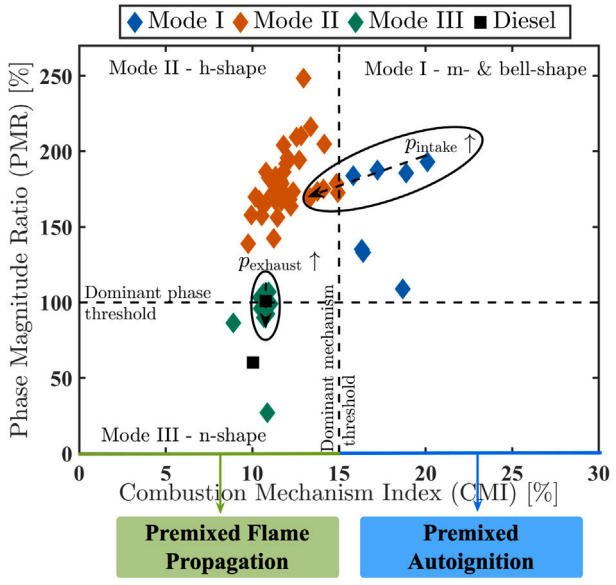

Fig. 17. Heat release profile mapping based on CMI and PMR metrics.

descriptors—the combustion mechanism index (CMI) and phase magnitude ratio (PMR)—were introduced to offer a morphological assessment of the HRR profiles. These metrics enabled systematic mapping and further classification of combustion behavior based on HRR shapes, as detailed in Section 3.3. The resulting map of Fig. 4 was then populated using the experimental data from the prior work. The first quadrant corresponds to m-shaped HRR profiles observed at relatively lower MEFs, defining Mode I, in which combustion is dominated by premixed autoignition of both diesel and methanol. With increasing MEF, the m-shape transitions to an h-shape, marked by lower CMI and higher PMR values. This shape change causes these combustion Mode II HRR profiles to populate quadrant II. At high MEFs and elevated intake temperatures, n-shaped profiles emerge, defining Mode III, at which energy release is primarily driven by methanol flame propagation, approaching spark-ignition-like behavior.

To extend this framework, this work quantifies the CMI and PMR metrics for the HRR profiles obtained from the intake and exhaust pressure sweeps, thereby populating the CMI-PMR map. The distribution of these HRR profiles across the pressure sweeps is illustrated in Fig. 17, alongside the investigated operating points of the preceding study. Across the intake pressure sweep, the HRR profile gradually evolves from a single-peak and “quasi-bell-shaped” profile to the double-peak h-shaped profile, as identified in [39]. Using the conceptual model in Fig. 8 of Section 4.1, this evolution is attributed to the increasingly distinct separation between the diesel and methanol combustion phases, leading to a less homogeneous overall combustion process. At lower intake pressures, the longer ID and higher reactivity of the methanol-air mixture promote greater methanol combustion under premixed autoignition within Stages I and II. This behavior aligns with the CMI-PMR trends, placing the lowest intake pressure conditions within the Mode I quadrant, which signifies premixed autoignition dominance.

However, the bell-shaped profile occupies a distinct region within the quadrant (blue diamonds in the circle of Mode I quadrant). Despite the elevated CMI metric, its PMR values remain elevated, higher than those associated with the m-shaped profiles. Although both profile types reflect a strong contribution of premixed autoignition to methanol combustion, the underlying source of this autoignition differs, resulting in their distinct HRR shapes and PMR magnitudes. For the bell-shaped profiles, the intensified premixed autoignition primarily originates from the longer ID at low intake pressure, which leads to a larger portion of methanol undergoing Stage I autoignition alongside the pilot diesel. In contrast, the premixed autoignition that characterizes the m-shaped profiles arises predominantly from an intensified Stage II process, clearly separated from the pilot diesel combustion of Stage I. Overall, the chosen CMI threshold of 15% effectively indicates the transition from premixed flame propagation toward an enhanced premixed autoignition as the governing methanol combustion.

For the exhaust pressure sweep, the influence on combustion morphology is comparatively weaker. Adjustments in exhaust pressure introduce only minor variations in the PMR metric, indicating a modest strengthening of Phase II relative to Phase I, with CMI remaining nearly constant. The corresponding operating points cluster near the boundary between Modes II and III quadrants of the combustion mode map. Moreover, these points are situated away from the mechanism-transition threshold and exhibit n-shaped HRR profiles, a characteristic of flame propagation-dominated combustion in the methanol-air mixture. On the whole, the integrated CMI-PMR analysis across all operating points underscores that boundary conditions beyond pilot injection timing—such as air excess ratio, intake temperature, and trapped residual gases—influence and can govern the balance between premixed autoignition and flame propagation mechanisms, dictating the combustion behavior and resulting heat release characteristics.

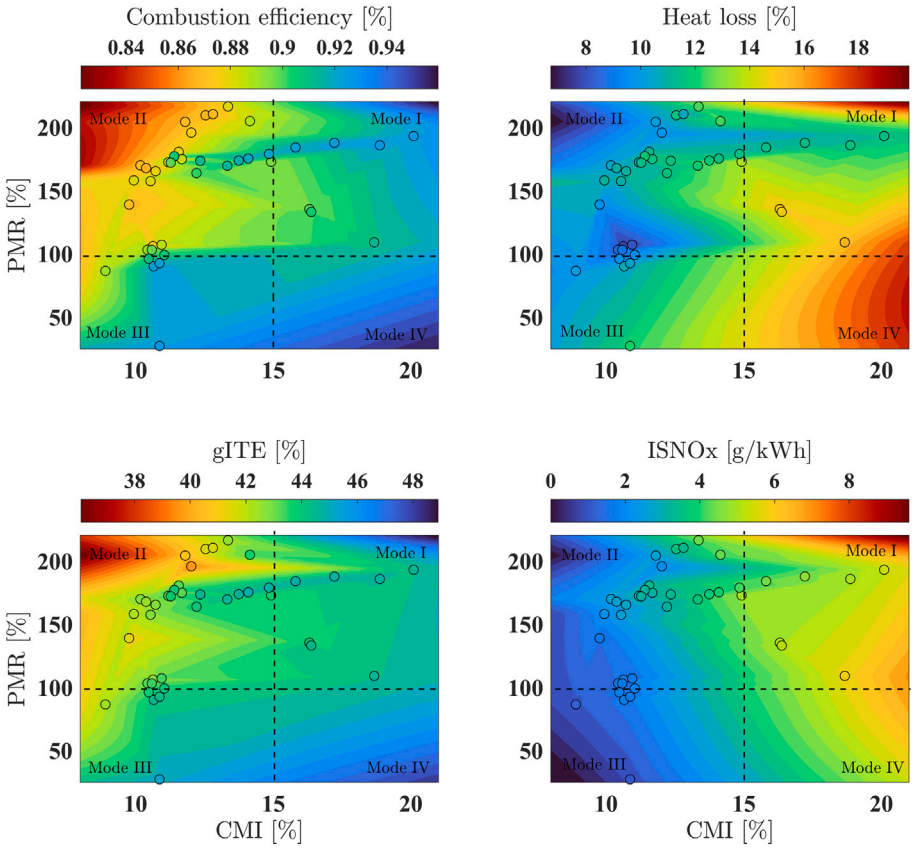

Fig. 18. Contours of key performance indicators over the CMI-PMR map.

To link heat release morphology to efficiency and emissions, Fig. 18 maps four key performance indicators—combustion efficiency, heat losses, gITE, and $ISNO_x$—in the CMI-PMR plane. Note that the lower-right quadrant (Mode IV) is not populated by any of the experimental data obtained in this study or the preceding one; hence, any contouring in that region should be interpreted with caution. Nevertheless, the dominant trends are clear. Combustion efficiency is lowest in Mode II, where h-shaped HRR profiles prevail. This is consistent with the mechanism translated by the CMI-PMR analysis: a pronounced separation between Phase I and the comparatively slow Phase II that deteriorates overall combustion efficiency. As CMI increases, signaling a shift toward stronger methanol premixed autoignition, combustion efficiency rises, with the highest values found in Mode I. Importantly, n-shaped profiles (Mode III) also deliver high combustion efficiency at more elevated MEF compared to Mode I cases. This enhanced combustion performance within a premixed flame propagation regime is achieved by tuning certain boundary conditions like intake temperatures to strengthen combustion Phase II.

Heat losses follow a broadly opposing trend to combustion efficiency; yet Mode I shows a consistent difference between m-shaped and bell-shaped curves. The m-shaped Mode I points exhibit higher heat losses than the bell-shaped Mode I points, primarily attributed to their lower MEF ($\approx$ 62% versus $\approx$ 81%) and the reduced cooling effect, thereby increasing bulk gas temperatures and wall heat transfer. Interestingly, the effect of combustion efficiency is dominant over heat losses, indicating that for PRDF methanol engines, design optimization should focus on increasing combustion efficiency. The increased combustion efficiency yields clear efficiency improvements, as indicated under both Mode I and III conditions. By contrast, the NO_x map shows a pronounced CMI-driven increase: transitioning from flame propagation-dominated to premixed autoignition-dominated combustion advances phasing toward TDC and elevates in-cylinder temperatures. These higher in-cylinder temperatures and the lower MEF in these cases result in increased NO_x formation. These results confirm that the CMI-PMR metrics not only classify combustion physics but also can summarize and clarify the direction of performance-emissions trade-offs, thereby offering an effective tool for boundary-condition tuning and control.

5. Conclusions

This study examined the isolated effects of intake and exhaust pressure conditions on the combustion dynamics and performance of a retrofitted single-cylinder, marine-scale methanol premixed dual-fuel (PRDF) engine operating at high load and high methanol energy fractions (MEFs). Building on a dual analytical framework developed in a preceding study, this work extends the understanding of how retrofit-friendly control levers influence combustion behavior in these methanol PRDF engines. The aim was to isolate specific boundary conditions—air excess ratio and residual gas (RG) mass—to provide insights applicable to control and optimization strategies for these engines. The main conclusions and recommendations are as follows:

- Intake pressure manipulation proves to be an effective strategy for enhancing combustion efficiency through air excess ratio control. Richer mixtures enabled significantly higher combustion efficiency, from 86.7 to 92.7% across the employed sweep, with only marginal increases in heat losses. This provides room for further improvements through complementary adjustments such as intake air temperature or pilot injection timing.
- Nitrogen dioxide (NO_2) emissions increase at lower intake pressure with richer mixtures. This is attributed to the higher concentration of hydroperoxyl (HO_2) radicals in the unburned zone combined with higher nitrogen monoxide (NO) species from the combustion zone.
- Although exhaust pressure adjustments demonstrate weaker influence on the heat release rate (HRR) profile compared to intake pressure, they yield a comparable improvement in combustion efficiency. The increase in trapped hot RGs promotes methanol combustion, particularly in the region away from the jets during the flame propagation stage (Stage III). This highlights that RG management, which can be accomplished with alternative control strategies, is a promising strategy to enhance combustion quality.
- Quantitative HRR morphology mapping across the two pressure sweeps reveals stronger sensitivity of the HRR profile to intake pressure. Increasing intake pressure induces a transition from a single-peak (bell-shaped) to a double-peak (h-shaped) profile, reflecting a shift in dominant combustion mechanisms from premixed autoignition to flame propagation.
- The combustion mechanism index (CMI)-phase magnitude ratio (PMR) map further demonstrates its capability to bridge combustion phenomena through heat release morphology to engine-level performance indicators. This mapping framework can be a very effective tool for boundary-condition tuning and combustion control, providing a lever for steering combustion toward a desirable efficiency-emissions trade-off.

Overall, this study underscores the potential of retrofit-friendly levers—such as intake and exhaust pressure control—to enhance combustion stability and efficiency in methanol PRDF engines at high MEFs and high loads. While optimization was not the focus of this work, the findings provide a strong foundation for future design-of-experiment (DOE) studies and control strategies aimed at improving performance and expanding the stable operating range of methanol-fueled PRDF systems.

CRediT authorship contribution statement

Konstantinos I. Kiouranakis: Writing – original draft, Visualization, Methodology, Investigation, Formal analysis, Data curation, Conceptualization. **Robbert Willems:** Writing – review & editing, Resources, Methodology, Investigation, Data curation, Conceptualization. **Peter de Vos:** Writing – review & editing, Supervision, Conceptualization. **Rinze Geertsma:** Writing – review & editing, Supervision, Project administration, Funding acquisition, Conceptualization.

Declaration of competing interest

The authors declare the following financial interests/personal relationships which may be considered as potential competing interests:

Konstantinos Ioannis Kiouranakis reports that financial support was provided by the Netherlands Enterprise Agency. If there are other authors, they declare that they have no known competing financial interests or personal relationships that could have appeared to influence the work reported in this paper.

Acknowledgements

The present work is part of the MENENS project (Methanol als Energiestap Naar Emissieloze Nederlandse Scheepvaart). The project is funded by the Netherlands Enterprise Agency (RVO: Rijksdienst voor Ondernemend Nederland) under the grant number MOB21012. Gratitude is extended to the TNO engine lab team for providing us with the opportunity to collaborate on this experimental research study. The author acknowledges the use of Perplexity AI as a supervisory tool for grammar and readability. The tool was applied carefully, solely sentence by sentence where necessary, to enhance clarity and language without altering the scientific content.

Data availability

Data will be made available on request.

References

[1] Verhelst S, Turner JWG, Sileghem L, Vancoillie J. Methanol as a fuel for internal combustion engines. Prog Energy Combust Sci 2019;70:43–88. https://doi.org/10.1016/j.pecs.2018.10.001

[2] Svanberg M, Ellis J, Lundgren J, Landälv I. Renewable methanol as a fuel for the shipping industry. Renew Sustain Energy Rev 2018;94:1217–28. https://doi.org/10.1016/j.rser.2018.06.058

[3] International Maritime Organization. MARPOL annex VI and NTC 2008 with guidelines for implementation. International Maritime Organization; 2023. https://doi.org/10.62454/KD664E. https://imo-epublications.org/content/books/9789280117523.

[4] Xing H, Stuart C, Spence S, Chen H. Alternative fuel options for low carbon maritime transportation: pathways to 2050. J Clean Prod 2021;297:126651. https://doi.org/10.1016/j.jclepro.2021.126651

[5] International Transport Forum. The potential of E-fuels to decarbonise ships and aircraft. International Transport Forum Policy Papers 111. 2023. https://doi.org/10.1787/3d96e0d9-en

[6] DNV. Maritime forecast to 2050. Technical Report; 2025. https://www.dnv.com/maritime/maritime-forecast/.

[7] International Chamber of Shipping. Fuelling the fourth propulsion revolution. Technical Report; 2022. https://www.ics-shipping.org/publication/fuelling-the-fourth-propulsion-revolution-an-opportunity-for-all-full-report/.

[8] Kiouranakis KI, Vos de P, Geertsma R, Methanol as a fuel in shipping: review and outlook to ICE research within MENENS. In: Transport transitions: advancing sustainable and inclusive mobility. Springer Nature Switzerland; 2025. pp. 735–42. https://doi.org/10.1007/978-3-031-89444-2_106. https://link.springer.com/10.1007/978-3-031-89444-2_106., series Title: Lecture Notes in Mobility.

[9] Kiouranakis KI, De Vos P, Zoumpourlos K, Coraddu A, Geertsma R. Methanol for heavy-duty internal combustion engines: review of experimental studies and combustion strategies. Renew Sustain Energy Rev 2025;214:115529. https://doi.org/10.1016/j.rser.2025.115529

[10] Dejaegere Q, Ballerini A, Demiddeleer S, Vanderbeken T, Bracke K, Gyselinck B, D'Errico G, Verhelst S. Assessment of a heavy-duty diesel engine retrofitted to dual-fuel and neat methanol SI operation. In: WCX SAE World Congress experience. Detroit, Michigan, United States; 2025. p. 2025–01–8440. https://doi.org/10.4271/2025-01-8440. https://www.sae.org/content/2025-01-8440.

[11] Wang Q, Wei L, Pan W, Yao C. Investigation of operating range in a methanol fumigated diesel engine. Fuel 2015;140:164–70. https://doi.org/10.1016/j.fuel.2014.09.067

[12] Suijs W, De Graeve R, Verhelst S. An exploratory study of knock intensity in a large-bore heavy-duty methanol engine. Energy Convers Manag 2024;302:118089. https://doi.org/10.1016/j.enconman.2024.118089

[13] Dominguez VM, Hernandez JJ, Ramos A. Role of the compression ratio in Dual-Fuel compression ignition combustion with hydrogen and methanol. Energy Fuels 2024;38. https://doi.org/10.1021/acs.energyfuels.4c02741

[14] Hountalas DT, Zannis TC, Mavropoulos GC. Potential benefits in heavy duty diesel engine performance and emissions from the use of variable compression ratio. In: SAE International Congress & Exhibition, Society of Automotive Engineers (SAE) at: Detroit, Michigan, U.S.A.volume: special publications SP-2012: compression ignition combustion process; 2006. p. 2006–01–0081. https://doi.org/10.4271/2006-01-0081. https://www.sae.org/content/2006-01-0081/.

[15] Bora BJ, Saha UK. Experimental evaluation of a rice bran biodiesel – biogas run dual fuel diesel engine at varying compression ratios. Renew Energy 2016. https://doi.org/10.1016/j.renene.2015.11.002

[16] Saxena MR, Maurya RK. Effect of premixing ratio, injection timing and compression ratio on nano particle emissions from dual fuel non-road compression ignition engine fueled with gasoline/methanol (port injection) and diesel (direct injection). Fuel 2017;203:894–914. https://doi.org/10.1016/j.fuel.2017.05.015

[17] Ott M, Buffart I, Schönbächler F, Teramoto J, Ataibi M. Compression without compromise: dynamic optimisation of combustion in dual-fuel engines with VCR. In: 29th Supercharging Conference. Zurich: CIMAC; 2025.

[18] Modiyani R, Kocher L, Van Alstine DG, Koeberlein E, Stricker K, Meckl P, Shaver G. Effect of intake valve closure modulation on effective compression ratio and gas exchange in turbocharged multi-cylinder engines utilizing EGR. Int J Engine Res 2011;12:617–31. https://doi.org/10.1177/1468087411415180

[19] Wu T, Yao A, Qu G, Ai Y, Wang W, Ma B, Yao C. Experimental study on ultra-low raw emissions in diesel/methanol dual fuel engine based on dual-loop EGR. E3S Web Conf 2022;360:01037. https://doi.org/10.1051/e3sconf/202236001037

[20] Tyrewala DS, Rothamer D, Ghandhi J. Assessing the influence of EGR on diesel pilot ignition combustion with methane/hydrogen blends in a single-cylinder compression ignition engine. Int J Engine Res 2025;26:1003–16. https://doi.org/10.1177/14680874241305837

[21] Dominguez V, Hernandez JJ, Ramos A, Reyes M, Rodriguez-Fernandez J. Hydrogen or hydrogen-derived methanol for dual-fuel compression-ignition combustion. Fuel 2023. https://doi.org/10.1016/j.fuel.2022.126301

[22] Wang Q, Yao C, Dou Z, Wang B, Wu T. Effect of intake pre-heating and injection timing on combustion and emission characteristics of a methanol fumigated diesel engine at part load. Fuel 2015;159:796–802. https://doi.org/10.1016/j.fuel.2015.07.032

[23] Li G, Zhang C, Li Y. Effects of diesel injection parameters on the rapid combustion and emissions of an HD common-rail diesel engine fueled with diesel-methanol dual-fuel. Appl Therm Eng 2016;108:1214–25. https://doi.org/10.1016/j.applthermaleng.2016.08.029

[24] Yang D, Wei S, Ma Y, J. E, Zhao J. Influence of critical parameters on combustion and emission characteristics of methanol/diesel dual fuel compression combustion engine. Fuel 2024;368:131647. https://doi.org/10.1016/j.fuel.2024.131647

[25] Srna A, Von Rotz B, Herrmann K, Boulouchos K, Bruneaux G. Experimental investigation of pilot-fuel combustion in dual-fuel engines, part 1: thermodynamic analysis of combustion phenomena. Fuel 2019;255:115642. https://doi.org/10.1016/j.fuel.2019.115642

[26] Srna A, Von Rotz B, Bolla M, Wright YM, Herrmann K, Boulouchos K, Bruneaux G. Experimental investigation of pilot-fuel combustion in dual-fuel engines, part 2: understanding the underlying mechanisms by means of optical diagnostics. Fuel 2019;255:115766. https://doi.org/10.1016/j.fuel.2019.115766

[27] Ma B, Yao A, Yao C, Chen C, Qu G, Wang W, al. E. Multiple combustion modes existing in the engine operating in diesel methanol dual fuel. Energy 2021;234:121285. https://doi.org/10.1016/j.energy.2021.121285

[28] Di Battista D, Di Bartolomeo M, Cipollone R. Flow and thermal management of engine intake air for fuel and emissions saving. Energy Convers Manag 2018. https://doi.org/10.1016/j.enconman.2018.07.074

[29] Wasberg H. Electrical heater for charge air conditioning on a research engine [BSc Thesis]. 2012. https://www.theseus.fi/handle/10024/43450.

[30] Cung K, Kalaskar V, Mitchell R, Wallace J, Briggs T, Smith E, Michlberger A, Williams DR, Bitsis C. Improved combustion efficiency in methanol/renewable diesel dual fuel combustion by advanced injection timing and increased intake temperature: single-cylinder experiment. In: Energy & propulsion conference & exhibition. Greenville, South Carolina, United States; 2023. p. 2023–01–1641. https://doi.org/10.4271/2023-01-1641.

[31] Varde KS. Ignition delay and emissions characteristics of a methanol-diesel fueled engine at low charge temperatures, 1992. https://doi.org/10.4271/920037

[32] Pan W, Yao C, Han G, Wei H, Wang Q. The impact of intake air temperature on performance and exhaust emissions of a diesel methanol dual fuel engine. Fuel 2015;162:10–101. https://doi.org/10.1016/j.fuel.2015.08.073

[33] Kumar D, Sonawane U, Chandra K, Agarwal AK. Experimental investigations of methanol fumigation via port fuel injection in preheated intake air in a single cylinder dual-fuel diesel engine. Fuel 2022;324:124340. https://doi.org/10.1016/j.fuel.2022.124340

[34] Dierickx J, Dejaegere Q, Van Gijzeghem A, Devos S, De Cock B, Verhelst S. Effect of intake conditions (temperature, pressure and EGR) on the operation of a dual-fuel marine engine with methanol. In: 16th international conference on engines & vehicles. Capri, Italy; 2023. p. 2023–24–0046. https://doi.org/10.4271/2023-24-0046. https://www.sae.org/content/2023-24-0046.

[35] Guan W, Wang X, Zhao H, Liu H. Exploring the high load potential of diesel–methanol dual-fuel operation with miller cycle, exhaust gas recirculation, and intake air cooling on a heavy-duty diesel engine. Int J Engine Res 2021;22:2318–36. https://doi.org/10.1177/1468087420926775

[36] Cung KD, Wallace J, Kalaskar V, Smith Iii EM, Briggs T, Bitsis Jr. DC. Experimental study on engine and emissions performance of renewable diesel methanol dual fuel (RMDF) combustion. Fuel 2024;357:129664. https://doi.org/10.1016/j.fuel.2023.129664

[37] Stenzel K, Thorau P, Beckmann L, Schirrmeister F, Reiser C, Buchholz B. Experimental investigations of a methanol dual-fuel combustion process for marine engines. CIMAC; 2025, Zurich.

[38] Splitter D, Szybist J, Jatana G, Svensson K, Montgomery D. Approach for high methanol substitution by energy with conventional and bio pilot fuels. CIMAC; 2025, Zurich.

[39] Kiouranakis KI, Willems R, De Vos P, Geertsma R. Combustion mode analysis of a large-bore methanol premixed dual-fuel engine with high methanol energy fractions. Energy Convers Manag X 2026;29:101417. https://doi.org/10.1016/j.ecmx.2025.101417

[40] Yun HJ, Mirsky W. Schlieren-Streak measurements of instantaneous exhaust gas velocities from a spark-ignition engine, 1974. https://doi.org/10.4271/741015

[41] Demuynck J, De Paepe M, Sileghem L, Vancoillie J, Verhelst S, Chana K. Applying design of experiments to determine the effect of gas properties on in-cylinder heat flux in a motored SI engine. SAE Int J Engines 2012;5:1286–99. https://doi.org/10.4271/2012-01-1209

[42] Woschni G. A universally applicable equation for the instantaneous heat transfer coefficient in the internal combustion engine, SAE Technical Paper 670931, 1967. https://doi.org/10.4271/670931

[43] Karim GA ed. Dual-Fuel diesel engines. 0 ed. CRC Press; 2015. https://doi.org/10.1201/b18163. https://www.taylorfrancis.com/books/9781498703093.

[44] Li W, Liu Z, Wang Z. Experimental and theoretical analysis of the combustion process at low loads of a diesel natural gas dual-fuel engine. Energy 2016;94:728–41. https://doi.org/10.1016/j.energy.2015.11.052

[45] Lee J, Chu S, Min K, Kim M, Jung H, Kim H, Chi Y. Classification of diesel and gasoline dual-fuel combustion modes by the analysis of heat release rate shapes in a compression ignition engine. Fuel 2017;209:587–97. https://doi.org/10.1016/j.fuel.2017.07.067

[46] Ahmad Z, Kaario O, Qiang C, Larmi M. Effect of negative valve overlap in a heavy-duty methanol-diesel dual-fuel engine: a pathway to improve efficiency. Fuel 2022;317:123522. https://doi.org/10.1016/j.fuel.2022.123522
[47] Zhao Y, Liu X, Kook S. Combustion mode evaluation of a methanol–diesel dual direct injection engine with a control of injection timing and energy substitution ratio. SAE Int J Engines 2024;18:03–18–01–0002. https://doi.org/10.4271/03-18-01-0002
[48] Ahmad Z, Kaario O, Qiang C, Vuorinen V, Larmi M. A parametric investigation of diesel/methane dual-fuel combustion progression/stages in a heavy-duty optical engine. Appl Energy 2019;251:113191. https://doi.org/10.1016/j.apenergy.2019.04.187
[49] Srna A, Bolla M, Wright YM, Herrmann K, Bombach R, Pandurangi SS, Boulouchos K, Bruneaux G. Effect of methane on pilot-fuel auto-ignition in dual-fuel engines. Proc Combust Inst 2019;37:4741–9. https://doi.org/10.1016/j.proci.2018.06.177
[50] Li Y, Li H, Guo H, Li Y, Yao M. A numerical investigation on NO_2 formation in a natural gas–diesel dual fuel engine. J Eng Gas Turbines Power 2018;140:092804. https://doi.org/10.1115/1.4039734